Excitation Energy Migration in A Dodecameric Porphyrin Wheel

In-Wook Hwang,† Dah Mee Ko, Tae Kyu Ahn, Zin Seok Yoon, and Dongho Kim*

Center for Ultrafast Optical Characteristics Control and Department of Chemistry, Yonsei University, Seoul 120-749, Korea

Xiaobin Peng, Naoki Aratani, and Atsuhiro Osuka*

Department of Chemistry, Graduate School of Science, Kyoto University, and CREST (Core Research for Evolutional Science and Technology) of Japan Science and Technology Agency, Kyoto 606-8502, Japan

Received: December 16, 2004; In Final Form: March 3, 2005

Intramolecular excitation energy hopping (EEH) time within a dodecameric porphyrin wheel **C6ZA**, in which six meso−meso linked zinc(II) diporphyrin (**Z2**) subunits are bridged by 1,3-phenylene spacers, is deduced by a Förster energy hopping model based on S_1-S_1 exciton−exciton annihilation and anisotropy depolarization. Under the assumption that the energy hopping sites are six **Z2** subunits, two different observables (e.g., exciton−exciton annihilation and anisotropy depolarization times) consistently give the EEH time of 4.0 ± 0.4 ps via 1,3-phenylene spacer of **C6ZA**, which is faster than 9.4 ps of linear **2Z2** (1,3-phenylene-linked zinc(II) tetraporphyrin). As a consequence, **C6ZA** serves as a well-defined two-dimensional model for a light-harvesting complex.

Introduction

Currently, much effort has been directed toward unraveling the energy transport phenomena occurring in natural light-harvesting complexes (LH1 and LH2).[1−3] In parallel with this, the mimicry of natural light-harvesting complexes has been continuously attempted by the covalent synthesis of various types of porphyrin or related pigment arrays with the goal of applying these arrays to artificial light-harvesting systems and molecular photonic devices.[4−13] The covalent approach has the advantages of robust stability and precise control in the spatial arrangement and connecting spacer. The design and synthesis of light-harvesting systems that rival those in photosynthesis has been an important issue, which may require an organization of many pigments per unit cell.

Inspired by the wheel-like architectures of photosynthetic pigments (LH1 and LH2),[14] particular attention has been focused on the construction of covalently linked cyclic porphyrin arrays,[15] which may aid the understanding of energy transfer mechanisms or find new applications as optoelectronic materials.[16] In the bacterial photosynthetic antennae of LH1 and LH2, photosynthetic tetrapyrrolic pigments are deliberately positioned in a wheel-like arrangement, hence manipulating the absorbed light energy through an intra-wheel excitation energy hopping (EEH) process. The peripheral antenna LH2 of photosynthetic purple bacteria forms two wheel-like structures: B800 with 9 bacteriochlorophyll *a* (Bchl *a*) molecules and B850 with 18 Bchl *a* molecules.[14] The structural complexity in the circular arrangement of 18 Bchls *a* is that they are not evenly distributed. They are composed of 9 Bchl *a* dimeric forms with Mg−Mg intradimer distance of 8.7 Å, whereas it is 9.7 Å between the adjacent dimeric units. These dimer units are strongly coupled to form exciton states, as a consequence of the close slipped cofacial arrangement. The remaining 9 Bchls *a* in B800 are located just beneath the 18 Bchls *a* wheel by forming a perpendicular ring. The Mg−Mg distance between B800 Bchls *a* is 21 Å, that is, Bchls *a* may be regarded as monomers and thus are only weakly interacting.

To mimic the overall structures of LH1 and LH2, we recently developed a dodecameric pophyrin wheel (**C6ZA**), in which six meso−meso linked zinc(II) diporphyrin (**Z2**) subunits are bridged by 1,3-phenylene spacers that are used to produce curvature of the array[17] (Scheme 1). Besides the circular arrangement, **C6ZA** is well-suited in mimicking the natural photosynthetic pigments, because **Z2** subunits are similar to the dimeric pigments in B850.[14] In the previous communication, we reported the preparation/characterization of **C6ZA** and the EEH process via the 1,3-phenylene spacer of **C6ZA** that was based on a femtosecond transient absorption anisotropy measurement. Despite this, a more systematic approach is needed to give comprehensive information about the EEH, such as the molecular morphology effect, *linear* versus *cyclic*, or the exciton coupling effect. In this study, we have employed two constituent porphyrin arrays (i.e., **Z2** and **2Z2** as references of **C6ZA**) and introduced the exciton−excition annihilation to further clarify the EEH in **C6ZA**.

To explore the EEH phenomena, the polarization change between the ground and excited states is examined via fluorescence anisotropy and pump−probe transient absorption anisotropy (TAA) measurements. While the nanosecond time-resolved fluorescence anisotropy provides relevant information about the EEH as well as the rotational diffusion motion, femtosecond TAA measurements give direct evidence about the EEH, because the initial localization of excitations in weakly coupled multichromophores gives rise to fast depolarization as the excitation energy is transferred. The observed exciton−exciton annihilation is also well-associated with the EEH, because this process is conceived as an incoherent energy hopping from the

* To whom correspondence should be addressed. E-mail: dongho@yonsei.ac.kr (D.K.), osuka@kuchem.kyoto-u.ac.jp (A.O.).

† Current address: Center for Polymers and Organic Solids, University of California at Santa Barbara, Santa Barbara, CA 93106, U.S.A.

10.1021/jp044274a CCC: $30.25
Published on Web 04/12/2005

SCHEME 1. Structures of *Meso-meso* Linked Zinc(II) Diporphyrin (Z2), 1,3-phenylene Linked Zinc(II) Tetraporphyrin (2Z2), 1,3-phenylene-bridged Zinc(II) Porphyrin Array (nZA), and Dodecameric porphyrin wheel (C6ZA)

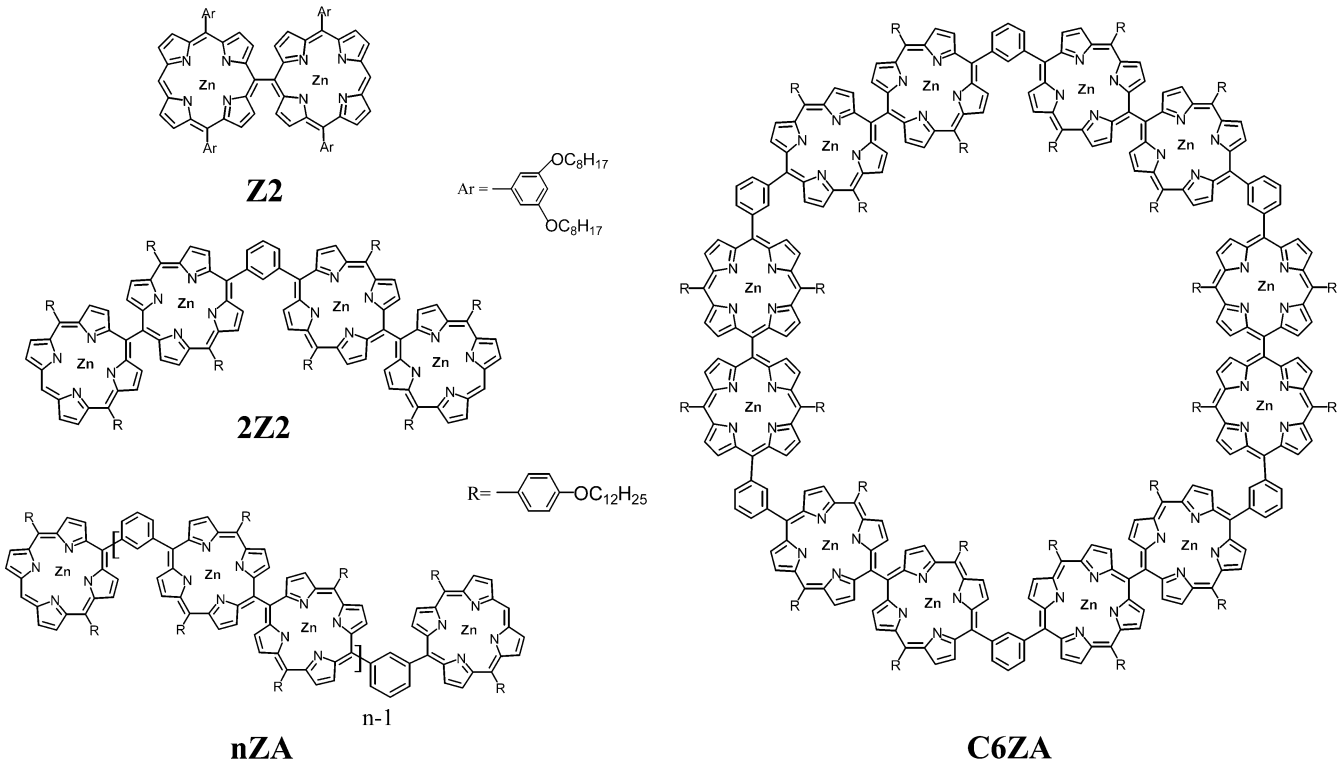

excited donor to the proximal excited acceptor.[15,18a] Using both the anisotropy depolarization and exciton−exciton annihilation times, we were able to quantify the EEH time over the cyclic **C6ZA**.

Experimental Section

Steady-State Spectra. The samples were prepared in approximately micromolar concentrations in tetrahydrofuran (THF). THF (~99.9% purity) was purchased from Merck Chemical Co. (HPLC grade). Absorption spectra were obtained with a Shimadzu model 1601 UV spectrometer, and steady-state fluorescence and fluorescence excitation spectra were measured by a Hitachi model F-2500 fluorescence spectrophotometer at room temperature. Steady-state excitation anisotropy spectra were obtained by changing the fluorescence detection polarization either parallel or perpendicular to the polarization of the excitation light. The excitation anisotropy spectra then were calculated as follows:

$$r = \frac{E_{VV} - GE_{VH}}{E_{VV} + 2GE_{VH}}$$

where E_{VV} (or E_{VH}) is the fluorescence excitation spectrum when the excitation light is vertically polarized and only the vertically (or horizontally) polarized portion of the fluorescence is detected, denoting that the first and second subscripts represent excitation and detection polarization, respectively. The factor G is defined by I_{HV}/I_{HH}, which is equal to the ratio of the sensitivities of the detection system for vertically and horizontally polarized light.

Fluorescence Decay and Fluorescence Anisotropy Decay. The time-correlated single photon counting (TCSPC) system was used for the fluorescence decay and fluorescence anisotropy decay measurements.[19] The system consisted of a self-mode-locked and cavity-dumped femtosecond Ti:sapphire laser pumped by a continuous wave (cw) Nd:YAG laser (Coherent, Verdi). The full width at half-maximum of the instrument response function obtained by a dilute solution of coffee cream was typically 50 ps in our TCSPC system. The fluorescence decays were measured with magic-angle emission polarization, and the number of fluorescence photons per unit time, detected by photomultiplier tube, was always maintained to <1% of the repetition rate of the excitation pulses, to prevent pile-up distortions in the decay profiles. Time-resolved fluorescence anisotropy decays were obtained by changing the detection polarization on the fluorescence path parallel or perpendicular to the polarization of the excitation light. The anisotropy decays then were calculated as follows:

$$r(t) = \frac{I_{VV}(t) - GI_{VH}(t)}{I_{VV}(t) + 2GI_{VH}(t)}$$

where $I_{VV}(t)$ (or $I_{VH}(t)$) is the fluorescence decay when the excitation light is vertically polarized and only the vertically (or horizontally) polarized portion of the fluorescence is detected, denoting that the first and second subscripts represent excitation and detection polarization, respectively. The factor G is defined by $I_{HV}(t)/I_{HH}(t)$, which is equal to the ratio of the sensitivities of the detection system for vertically and horizontally polarized light. The fittings for both isotropic and anisotropic decays were performed by a least-squares deconvolution fitting process.[20] The vertical and horizontal components of fluorescence emission were simultaneously fitted to extract an anisotropy decay function with an iterative nonlinear least-squares deconvolution procedure.

Femtosecond Transient Absorption and Transient Absorption Anisotropy. The dual-beam femtosecond time-resolved transient absorption spectrometer consisted of a self-mode-locked femtosecond Ti:sapphire oscillator (Coherent, MIRA), a Ti:sapphire regenerative amplifier (Clark MXR model

TRA-1000) that was pumped by a Q-switched Nd:YAG laser (Clark MXR model ORC-1000), a pulse stretcher/compressor, an optical parametric amplifier (Clark MXR OPA), and an optical detection system. A femtosecond Ti:sapphire oscillator pumped by a cw Nd:YVO_4 laser (Coherent, Verdi) produces a train of ~80-fs mode-locked pulses with an averaged power of 650 mW at 800 nm. The amplified output beam regenerated by chirped pulse amplification (CPA) had a pulse width of ca. 150 fs and a power of ca. 1 W at a repetition rate of 1 kHz, which was divided into two parts by a 1:1 beam splitter. One part was color-tuned for the pump beam by optical parametric generation and amplification (OPG-OPA). The resulting laser pulse had a temporal width of ~150 fs in the vis/IR range. The pump beam was focused to a spot diameter of ~1 mm, and the laser fluence was adjusted, using a variable neutral-density filter. The other part was focused onto a flowing water cell to generate a white-light continuum, which was again split into two parts. One part of the white-light continuum was overlapped with the pump beam at the sample to probe the transient, while the other part of the white-light continuum was passed through the sample without overlapping the pump beam. The time delay between pump and probe beams was controlled by making the pump beam travel along a variable optical delay line. The white-light continuum beams after the sample were sent through an appropriate interference filter and then were detected by two photodiodes. The outputs from the two photodiodes at the selected wavelength were processed by a combination of a boxcar averager and a lock-in amplifier, to calculate the absorption difference at the desired time delay between pump and probe pulses. For the transient absorption anisotropy decay $r(t)$, the probe white-light continuum pulse was set to have vertical polarization using a sheet polarizer. The excitation pulse then was changed to have parallel or perpendicular polarization by rotating a half-wave plate with respect to the polarization of the probe pulse. Finally, the transient absorption anisotropy decay was obtained by the following equation

$$r(t) = \frac{\Delta A_{VV}(t) - \Delta A_{HV}(t)}{\Delta A_{VV}(t) + 2\Delta A_{HV}(t)}$$

where the variables represent amplitudes. The fitting for the anisotropic decay was performed by a least-squares deconvolution fitting process with a trace of 150-fs pump pulse. The vertical and horizontal components of transient absorption (TA) decay were simultaneously fitted to extract an anisotropy decay function.

Results

Construction of C6ZA. In the previous work,[17] we reported the synthesis and characterization of **C6ZA**, where we attempted the intramolecular cyclization of the linear porphyrin 12mer **6ZA** (Scheme 1). Under very dilute conditions (9×10^{-7} M), **6ZA** was treated with 0.5 equiv of $AgPF_6$ for 48 h at room temperature. Progress of the reaction was monitored by analytical GPC−HPLC, which revealed the formation of a discrete product that eluted as a shoulder at 12.3 min, later than **6ZA** (11.9 min). This product, isolated by repeated preparative GPC−HPLC in 12% yield together with the recovery of **6ZA** (51%), was assigned to a wheel-like dodecameric porphyrin array, **C6ZA**, on the basis of the following facts: (1) The product exhibits the parent ion peak at 1167 (calcd for $C_{708}H_{816}N_{48}O_{24}Zn_{12}$, m/z = 1167) in MALDI-TOF mass, indicating its dodecameric porphyrin constitution. (2) Despite a small difference in the molecular weight, a distinct difference in the retention time on GPC−HPLC from **6ZA** indicates a substantial difference in the hydrodynamic volume, which may arise from an overall drastic change in molecular shape. (3) The ^{1}H NMR spectrum is quite simple, featuring only a single set of a porphyrin subunit without the edge meso-protons. (4) Finally, the scanning tunneling microscopy (STM) image exhibits a clear wheel-like structure.

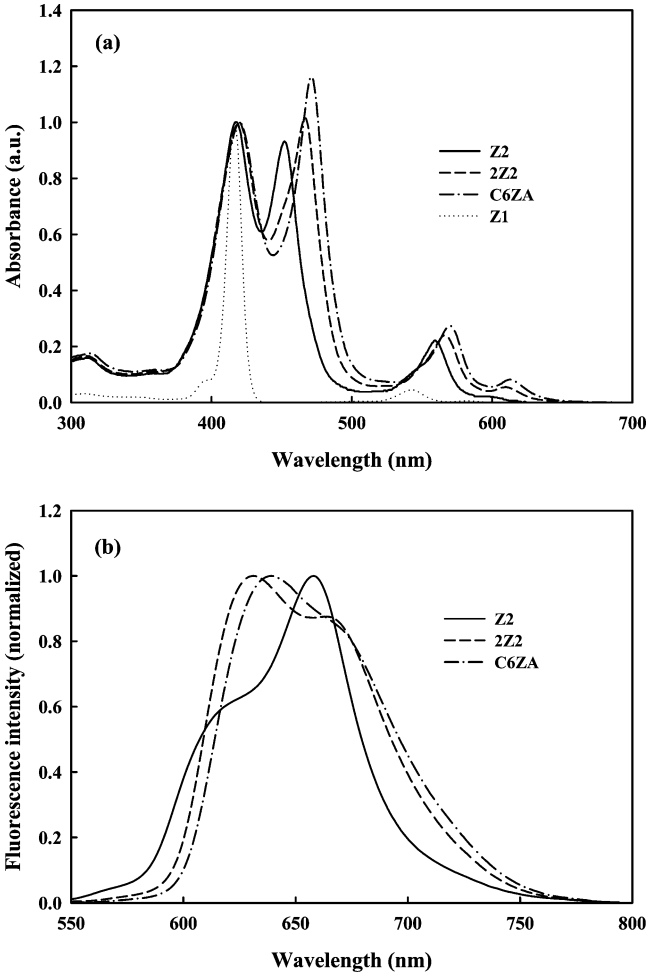

Figure 1. Steady-state (a) absorption and (b) fluorescence spectra of **Z2**, **2Z2**, and **C6ZA** in THF, to which the absorption spectrum of zinc(II) 5,15-bis(3,5-bis(octyloxy)phenyl)porphyrin (**Z1**) was added for comparison. The fluorescence spectra were obtained with the excitation wavelength 420 nm, on which the excitation wavelength dependence was negligible.

TABLE 1: Band Maxima in Absorption and Fluorescence Spectra of Z2, 2Z2, and C6ZA

	absorption (nm)				fluorescence (nm)[a]	
sample	Soret (high)	Soret (low)	$Q(1,0)$	$Q(0,0)$	$Q(0,0)$	$Q(0,1)$
Z2	417	452	559	598	612	658
2Z2	419	467	567	610	631	667
C6ZA	420	471	570	613	639	674

[a] The excitation wavelength of 420 nm was used.

Absorption, Fluorescence, and Fluorescence Excitation Anisotropy. Figure 1 shows the absorption and fluorescence spectra of **Z2**, **2Z2**, and **C6ZA** in THF, of which the peak positions are tabulated in Table 1. With an increase in the number of porphyrin units, the low-energy Soret band shifts to red, while the high-energy Soret band locates nearly at the same position as that of **Z1**, resulting in a progressive increase of the

SCHEME 2. Exciton Coupling in Z1, Z2, 2Z2, and C6ZA

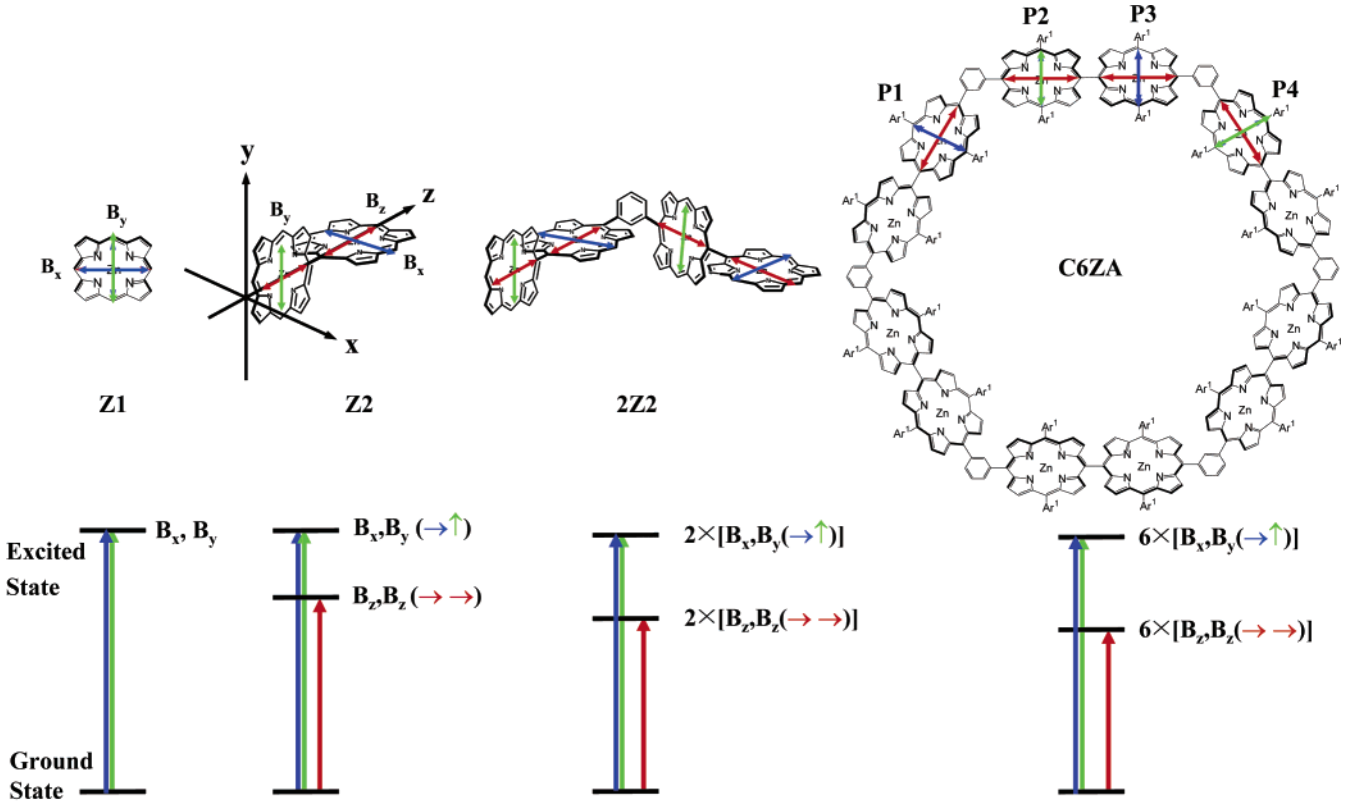

splitting energy in the order **Z2** < **2Z2** < **C6ZA**. While the split Soret bands of **Z2** are characteristic of excitonic dipole−dipole coupling between zinc(II) porphyrin monomers,[9c,d] the further split Soret bands of **2Z2** and **C6ZA** indicate additional dipole−dipole interaction between **Z2** subunits via the 1,3-phenylene spacer (Scheme 2 and Discussion section). In sharp contrast, the fluorescence and *Q*-absorption bands reveal relatively small red shifts in going from **Z2** to **2Z2** and **C6ZA**, indicating weak excitonic/electronic interaction between neighboring **Z2** units. In Figure 1, the *Q* band is undergoing the same red-shift as the Soret exciton band, but with a smaller magnitude because of a smaller transition dipole.[9c] In addition, the relative intensities of *Q*(1, 0) and *Q*(0, 0) bands increase going from **Z2** to **2Z2** and **C6ZA**, which also occurs in the Soret exciton band and concomitantly reflects increased dipole coupling as the array becomes longer.

The steady-state fluorescence excitation anisotropy spectra monitored at 625 nm are comparatively displayed for **Z2**, **2Z2**, and **C6ZA** in THF (Figure 2). The excitation anisotropy measurement is informative for the angle difference between absorption and emission dipoles as well as the EEH. The three molecules consistently reveal the profile exhibiting negative anisotropy in the high-energy Soret band and positive anisotropy in the low-energy Soret and *Q* bands. The negative anisotropy in the high-energy Soret band indicates orthogonal geometry as well as the EEH between porphyrin monomers within the **Z2** unit, in view of our previous reports[9c,d] on the orthogonally linked zinc(II) porphyrin arrays (**Z*n***). The absolute anisotropy value increases going from **Z2** to **2Z2**, revealing slow rotational diffusion motion in **2Z2**, while it decreases going from **2Z2** to **C6ZA**, indicating plausible excitation energy migration along the wheel. The excitation energy transfer between the same molecular units with different orientations generally gives rise to small fluorescence excitation anisotropy, resulting from new depolarization channels.[18a,b]

Fluorescence Lifetime and Fluorescence Anisotropy Decay. The time-resolved fluorescence decays of **Z2**, **2Z2**, and **C6ZA** are measured in THF (Figure 3), and their fitted fluorescence lifetimes are tabulated in Table 2. The fluorescence decay profiles exhibit single exponential decays, and their lifetimes are all similar with the exception of slight shortening going from **Z2** to **2Z2** and **C6ZA**. These results imply that the S_1 state of the **Z2** subunit is negligibly changed by the conformation motion of **C6ZA**. As a consequence, the long-lived S_1 state lifetime reflects an avoidance of energy sinks, which is an important requirement in the EEH.

The fluorescence anisotropy decay profiles of **Z2**, **2Z2**, and **C6ZA** are also measured in THF, where the excitation of the high-energy Soret band (i.e., λ_{ex} = 420 nm) was used (Figure 4). The fitted anisotropy decay parameters are listed again in Table 2. The fluorescence anisotropy decay times (Φ's) are well-associated with the molecular volumes, exhibiting the molecular rotational diffusion motion in THF, for which the rotational diffusion time increases going from **Z2** (0.87 ns) to **2Z2** (1.88 ns), and jumps to 6.6 ns in **C6ZA**. The fluorescence anisotropy decays consistently reveal negative amplitudes, in agreement with the negative anisotropies at the high-energy Soret bands of the steady-state excitation anisotropy spectra (see Figure 2). The excitation of the high-energy Soret band is known to induce coherent energy hopping within the **Z2** unit, which gives rise to a negative fluorescence anisotropy.[9c,d] Finally, the fitted anisotropy decay parameters suggest the EEH process via the 1,3-phenylene spacer. The initial $|r_0|$ value listed in Table 2 becomes small going from **Z2** (−0.03) to **2Z2** (−0.024) and **C6ZA** (−0.013), reflecting fast depolarization channels presumably due to the EEH via the 1,3-phenylene spacer, which cannot be resolved in the TCSPC system.

Femtosecond Transient Absorption and Transient Absorption Anisotropy. To explore the fast EEH, femtosecond TA and TAA measurements were conducted on **Z2**, **2Z2**, and

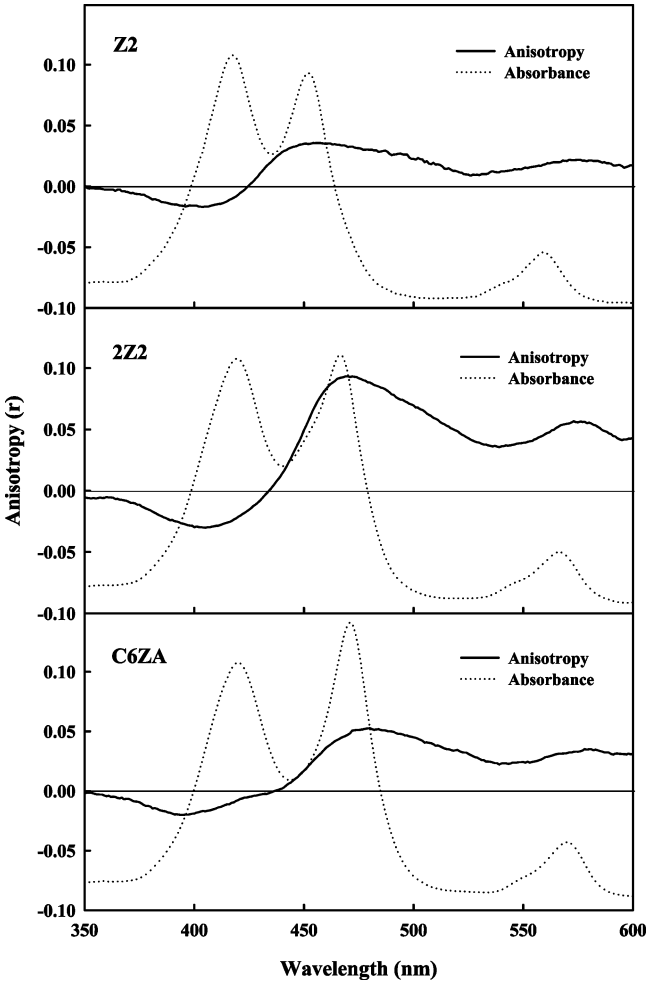

Figure 2. Steady-state fluorescence excitation anisotropy spectra of **Z2**, **2Z2**, and **C6ZA** in THF, in which the absorption spectra are included as dotted lines. The polarized excitation spectra (E_{VV} and E_{VH}) were measured at the emission wavelength of 625 nm, and then, the anisotropy spectra were calculated.

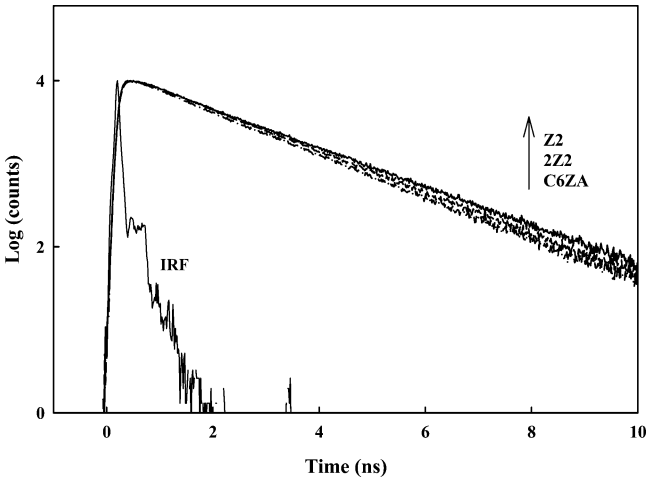

Figure 3. Time-resolved fluorescence decay profiles of **Z2**, **2Z2**, and **C6ZA** in THF, where the excitation wavelength of 420 nm and emission wavelength of 625 nm were used. IRF represents the instrument response function of our TCSPC system.

C6ZA, where the *Q*-band excitation (λ_{pump} = 575 nm) was employed to avoid an involvement of S_2-S_1 relaxation in the porphyrin (Figures 5−7). Figure 5 reveals the transient absorption spectra of **C6ZA** that are measured with time delays of a few picoseconds. As displayed, both bleaching recovery and induced-absorption signals of **C6ZA** show a TA decay component in the time region of a few picoseconds, for which **Z2** and **2Z2** do not show such decay component.

With the pump-power dependence on the TA decay, we were able to clarify the EEH in **C6ZA**. While **Z2** and **2Z2** reveal no power dependence on the TA decay with only slow decay components that are in agreement with the S_1 state lifetimes

TABLE 2: Fitted Fluorescence Lifetimes and Anisotropy Decay Parameters of Z2, 2Z2, and C6ZA in THF[a]

	fitted fluorescence lifetime[b]	anisotropy decay parameters[d]	
sample	τ (ns)[c]	r_0 [e]	Φ (ns)[e]
Z2	1.82 ± 0.01 (100%)	−0.030 ± 0.005	0.87 ± 0.18
2Z2	1.73 ± 0.01 (100%)	−0.024 ± 0.006	1.88 ± 0.41
C6ZA	1.66 ± 0.02 (100%)	−0.013 ± 0.004	6.60 ± 1.05

[a] The excitation wavelength, 420 nm, was applied to all experiments. [b] The fluorescence lifetimes of the samples were obtained by averaging the fitted single fluorescence lifetimes at several emission wavelengths. [c] Using the relation $I(t) = A\exp(-t/\tau)$, where $I(t)$ is the time-dependent fluorescence intensity, A the amplitude (noted in parentheses as the percentage), and τ the fitted fluorescence lifetime, the χ^2 values of the fittings were maintained at ∼1.0−1.3. [d] The fluorescence anisotropy decays were monitored at λ_{em} = 670 nm. [e] Using the relation $r(t) = r_0\exp(-t/\Phi)$, where $r(t)$ is the time-dependent fluorescence anisotropy $\{r(t) = [I_{\parallel}(t) - GI_{\perp}(t)]/[I_{\parallel}(t) + 2GI_{\perp}(t)]\}$, r_0 the initial anisotropy value, and Φ the fitted anisotropy decay time.

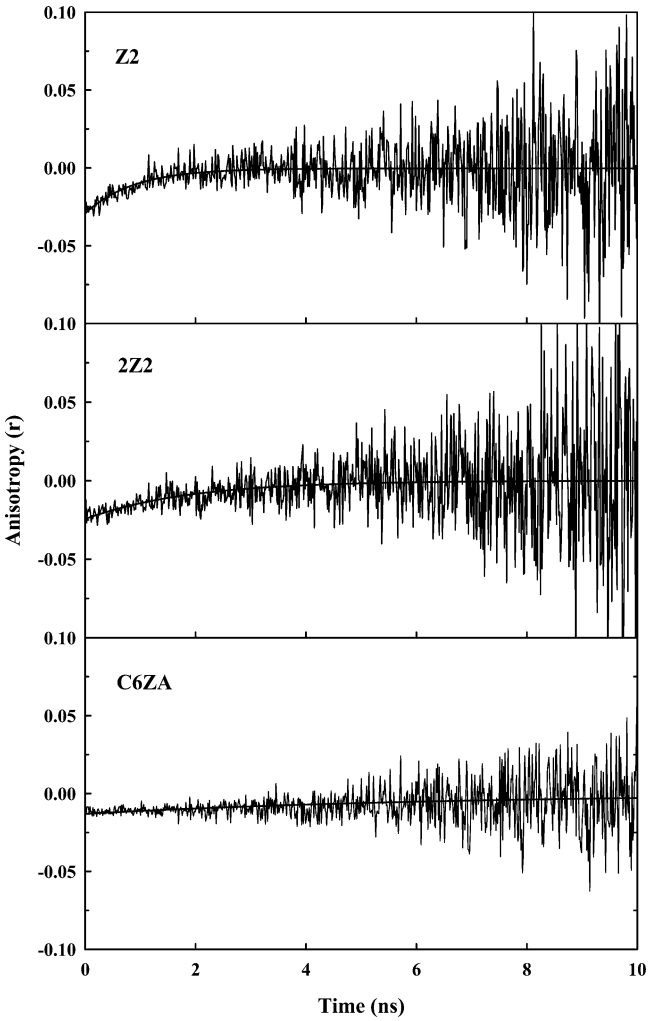

Figure 4. Time-resolved fluorescence anisotropy decay profiles of **Z2**, **2Z2**, and **C6ZA** in THF. The polarized fluorescence decays ($I_{VV}(t)$ and $I_{VH}(t)$) were measured using the excitation wavelength of 420 nm and emission wavelength of 625 nm, and then, the anisotropy decay $r(t)$ was calculated.

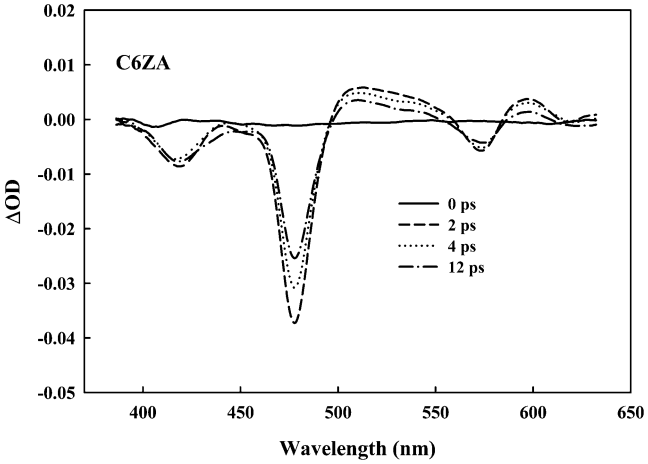

Figure 5. Transient absorption spectra of **C6ZA** in THF, in which the excitation wavelength of 575 nm and pump power of 2.0 mW were used.

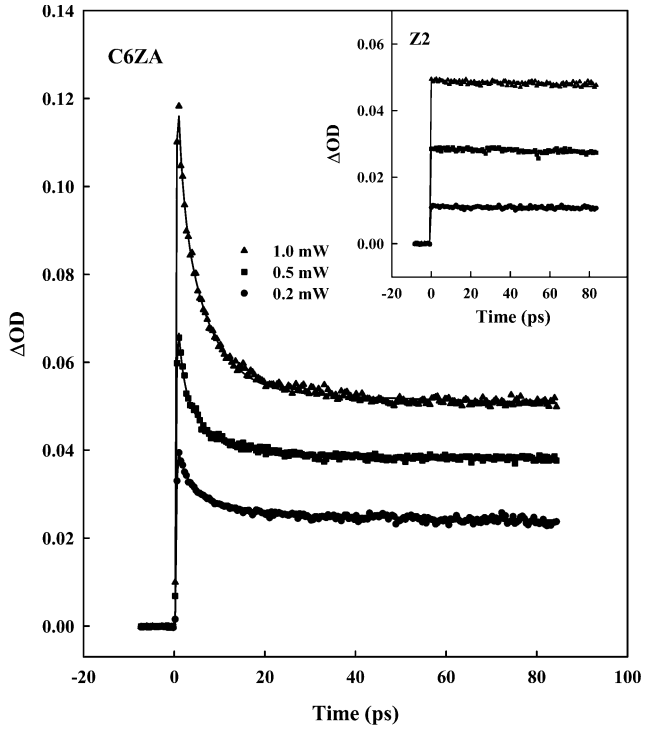

Figure 6. Transient absorption decay profiles of **C6ZA** that include pump-power dependence. The transient absorption decay profile of **Z2** is inserted (right). In the experiments, the pump and probe wavelengths were 575 and 510 nm, which are the *Q*-band excitation and induced-absorption probe, respectively. The solvent used was THF.

found in the TCSPC measurements (i.e., 1.82 and 1.73 ns for **Z2** and **2Z2**, respectively), the TA decay of **C6ZA** is very sensitive to the pump power (Figure 6 and Table 3). When the pump power is increased, the contributions of relatively fast τ_1 (1.1 ps) and τ_2 (6.2 ps) components are enhanced, as compared to the slowest τ_3 (1660 ps) one (Table 3, amplitudes). The pump-power dependence on the TA decay is a strong indication of S_1-S_1 exciton−exciton annihilation,[15,18a] because the intense excitation or high density of photons may generate two or more excitons in one cyclic array, and then, the recombination between excitons gives rise to a fast deactivation channel. According to the description on a natural light-harvesting system (LH1 and LH2), the exciton−exciton annihilation is conceived as a Förster-type incoherent energy hopping from the excited donor to the proximal excited acceptor unit resulting in a doubly

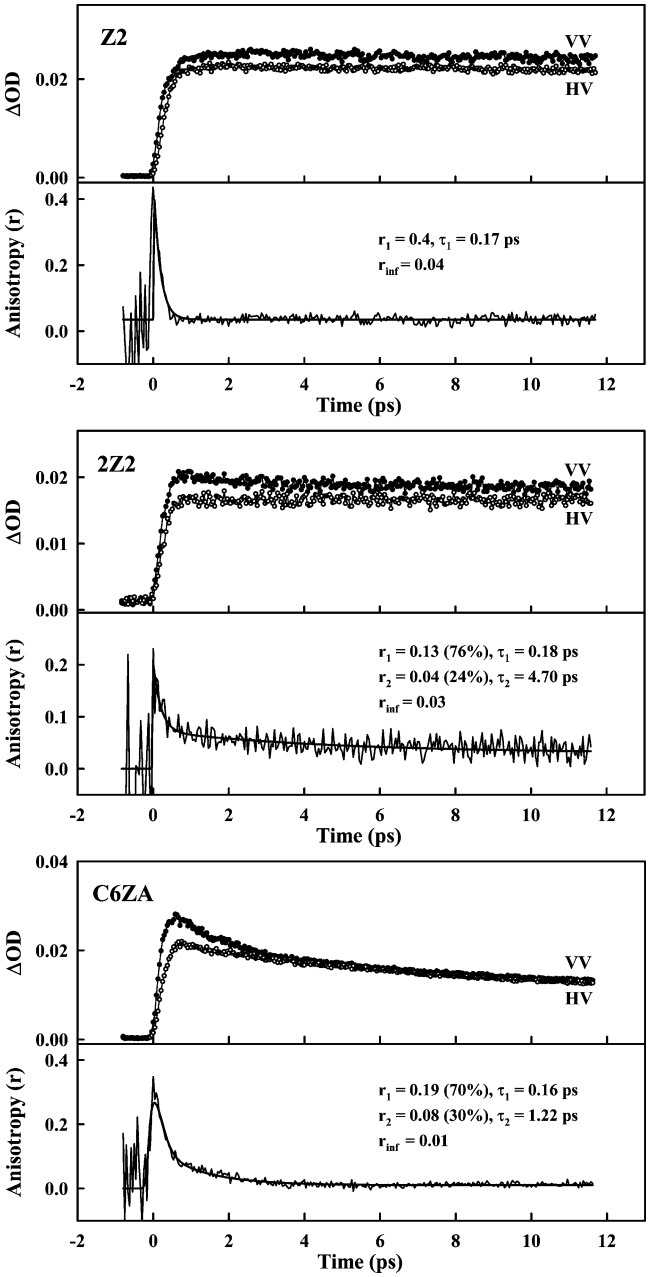

Figure 7. Transient absorption anisotropy decay profiles of **Z2**, **2Z2**, and **C6ZA** in THF, where the polarized transient absorption decays for parallel (VV) and perpendicular (HV) orientations between pump and probe beams are included in each panel. Insets show the deconvolution fitted anisotropy decay parameters with a train of 150-fs pump pulse. The pump and probe wavelengths were 575 and 510 nm, which are *Q*-band pump and induced-absorption probe.

excited acceptor state; the latter quickly relaxes to the singly excited state.[21,22]

Figure 7 reveals the TAA decay profiles of **Z2**, **2Z2**, and **C6ZA** that reflect fast depolarization channels, presumably because of the EEHs within the samples. While **Z2** shows a single TAA decay component with a time constant of 0.17 ps, the TAA decay of **2Z2** is fitted with two decay components (0.18 and 4.70 ps) where the fast component is similar to that of **Z2**. While the fast τ_1 components may come from the EEH between **Z1** units via direct linkage of **Z2**,[9d] the slow τ_2 component results from the EEH between **Z2** subunits via the 1,3-phenylene spacer of **2Z2**. On the contrary, **C6ZA** shows relatively fast TAA decay components ($\tau_1 = 0.16$ ps and $\tau_2 = 1.22$ ps), reflecting fast depolarization arising from the excitation

TABLE 3: Transient Absorption Decay Parameters for Z2, 2Z2, and C6ZA in THF[a]

pump power (mW)	fitted decay time (ps)[b]		
	τ_1	τ_2	τ_3
	Z2		
1.0	1820 (100%)		
0.5	1820 (100%)		
0.2	1820 (100%)		
	2Z2		
1.0	1730 (100%)		
0.5	1730 (100%)		
0.2	1730 (100%)		
	C6ZA		
1.0	1.1 (22%)	6.2 (38%)	1660 (40%)
0.5	1.1 (20%)	6.2 (22%)	1660 (58%)
0.2	1.1 (14%)	6.2 (18%)	1660 (68%)

[a] The pump and probe wavelengths are 575 and 510 nm, respectively. [b] Using the relation $\Delta OD(t) = A_1 \exp(-t/\tau_1) + A_2 \exp(-t/\tau_2) + A_3 \exp(-t/\tau_3)$, where $\Delta OD(t)$ is the transient absorption intensity, A the amplitude (noted in parentheses as the normalized percentage, i.e., $[A_i/(A_1 + A_2 + A_3)] \times 100$), and τ the fitted decay time.

energy migration along the wheel. In view of energy hopping dynamics, the fast τ_1 component of **C6ZA** is due to the depolarization inside the **Z2** subunit, because a similar time constant (<0.2 ps) was observed in reference to **Z2**. On the other hand, the slow τ_2 component is responsible for the EEH via the 1,3-phenylene spacer of **C6ZA**, because the comparable time constant (4.70 ps) was also observed in reference to **2Z2**.

Overall, it should be noted that there is a discrepancy between the TAA decay times (0.16 and 1.22 ps) and the exciton−exciton annihilation times (1.1 and 6.2 ps) of **C6ZA**. This discrepancy, however, is often found in other multi-chromophore systems (LH1 and LH2).[21,22] In a multi-chromophore system, neither exciton−exciton annihilation nor anisotropy depolarization time directly represents the EEH time between the adjacent hopping units, because they do not occur in a single donor−acceptor pair. The EEH time can only be theoretically obtained by modeling the EEH and the simultaneous use of these two observables.[21,22]

Discussion

Rotational Diffusion in THF. Rotational diffusion of molecules is a dominant cause of fluorescence depolarization that can be described by the Perrin equation[23]

$$r_o/r = 1 + \tau/\theta = 1 + 6D\tau \quad (1)$$

where τ is the fluorescence lifetime, θ the rotational correlation time, and D the rotational diffusion coefficient. Assuming a spherical molecule, the time-resolved anisotropy decay $r(t)$ is a single exponential

$$r(t) = r_o \exp[-t/\theta] = r_o \exp[-6Dt] \quad (2)$$

In eq 2, the rotational correlation time (θ) is given by

$$\theta = \eta V/RT \quad (3)$$

where η is the viscosity, T the temperature in Kelvin, R the gas constant, and V the volume of the rotating unit. The rotational correlation time is related to the rotational diffusion coefficient by $\theta = (6D)^{-1}$. Because the rotational diffusion time (τ_{rot}) is the rotational correlation time per molecule, τ_{rot} is given by

$$\tau_{rot} = \eta V/k_B T \quad (4)$$

where k_B is the Boltzmann constant. Because the rotational diffusion time is associated with the overall molecular structure (i.e., the molecular hydrodynamic volume), we evaluated the molecular volumes of **Z2**, **2Z2**, and **C6ZA** in THF. First, all the molecules were geometry optimized by MM^+ calculation, and then, their volumes were evaluated by the solvent probe radius of 2.64 Å that was estimated by calculating the volume of THF based on van der Waals surface interactions. Consequently, the molecular volumes were estimated to be 9028, 17 136, and 42 915 Å^3 for **Z2**, **2Z2**, and **C6ZA**, respectively, which give rise to the rotational diffusion times of 1.23, 2.33, and 5.83 ns when the viscosity $\eta = 0.55$ cp was employed for THF. The calculated rotational diffusion times are well-associated with the experimental values (0.87, 1.88, 6.6 ns) that were found in the fluorescence anisotropy decay measurements (Figure 4 and Table 2). In the calculation, we assumed spherical molecules, because the long alkyl substituents (3,5-bis(octyloxy)phenyl) and orthogonal arrangements between the porphyrin units led to three-dimensional sphere-like architectures rather than disklike ones, despite linear or disklike porphyrin assemblies drawn in Scheme 1.

Excitonic Dipole−Dipole Coupling. The absorption spectra of **Z2**, **2Z2**, and **C6ZA** are explained in terms of exciton coupling theory (Scheme 2). The Soret band of the porphyrin monomer (**Z1**) has two perpendicular transition dipole moments B_x and B_y that are degenerate. In the orthogonally linked zinc(II) diporpyrin **Z2**, two transition dipole moments B_z and B_z are coupled as J-aggregates giving rise to a red-shifted band (low-energy Soret band), while B_x and B_y do not couple because of mutual orthogonal geometry, resulting in the same band position (high-energy Soret band) as that of **Z1** (Figure 1 and Scheme 2).[9c,d] The low-energy Soret band is further red-shifted, because of additional exciton coupling via 1,3-phenylene spacers of **2Z2** and **C6ZA**. The dipole moments of **2Z2** and **C6ZA** consist of the dipole moments (B_x, B_y) perpendicular to B_z along the long axis (*z*-axis). These dipole moments are coupled in a manner similar to that of **Z2**. For the B_z components, the in-phase arrangement of transition dipoles is attractive and leads to a lowering of energy, while the dipole couplings between B_x and B_y components cannot occur because of orthogonal geometries (Scheme 2).

According to the point−dipole approximation,[24] the excitonic coupling strength between adjacent dipole moments is given by where the angles define the relative in-plane (θ_i) and out-of-plane (φ) orientations between the transition dipole moments *A* and *B*. With the geometry optimization of **Z2** and **2Z2** (MM^+ force field), the center-to-center distance (R_{ij}) and angles (θ_i and φ) between B_z dipoles were determined as $R = 7.95$ Å, $\theta_1 = 0°$, $\theta_2 = 180°$, and $\phi = 0°$ for the direct linkage of **Z2** and $R = 10.07$ Å, $\theta_1 = 34.79°$, $\theta_2 = 145.21°$, and $\phi = 3.56°$ for the 1,3-phenylene linkage of **2Z2**. Using the reported dipole strength (9.5 ± 0.5 D)[25] of the Soret band of zinc(II) porphyrin monomer, we were able to calculate the exciton coupling strengths between the porphyrin units, where it is only needed to evaluate the coupling strength between B_z dipoles, because

$$V_{AB} = \frac{|\mu_A \mu_B|}{4\pi\epsilon_0 R^3}(2\cos\theta_A \cos\theta_B + \sin\theta_A \sin\theta_B \cos\varphi) \quad (5)$$

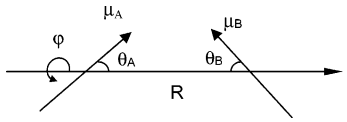

the interaction between B_x and B_y should be zero, owing to their averaged perpendicular conformation. As a consequence, the coupling strength between adjacent B_z dipoles via meso−meso direct linkage is calculated to be 1806 cm^{-1}, which is consistent with the experimental Soret band split (1857 cm^{-1}) of **Z2**, while the coupling strength between neighboring B_z dipoles bridged by the 1,3-phenylene spacer is calculated to be 455 cm^{-1}. In the cases of **2Z2** and **C6ZA**, the total excitonic coupling strength is the summation of the excitonic coupling strength between adjacent porphyrin monomers within the **Z2** unit and that between neighboring porphyrin monomers bridged by the 1,3-phenylene spacer as described below

$$V = V_{P1,P2} + V_{P2,P3} \text{ for } \mathbf{2Z2} \tag{6a}$$

$$V = V_{P1,P2} + V_{P2,P3} + V_{P3,P4} \text{ for } \mathbf{C6ZA} \tag{6b}$$

where $V_{Pi,Pj}$ denotes the dipole coupling strength between porphyrin moieties Pi and Pj within **2Z2** and **C6ZA** (Scheme 2, right). In our calculations, the nonnearest dipole couplings between porphyrin moieties either directly coupled or 1,3-phenylene-linked were not considered because of their small contributions. In addition, we assumed a simple sum of the interaction of the single porphyrin with its nearest neighbors, because the regarded interaction between multi-porphyrins such as two **Z2** moieties gave rise to values with much larger errors. Consequently, the coupling strengths of $V_{P1,P2} = 455$ cm^{-1} and $V_{P2,P3} = 1806$ cm^{-1} result in the total coupling strength of 2261 cm^{-1} in **2Z2**, which is in good agreement with the experimental Soret band split (2453 cm^{-1}). In a similar manner, the coupling strengths of $V_{P1,P2} = 455$ cm^{-1}, $V_{P2,P3} = 1806$ cm^{-1}, and $V_{P3,P4} = 455$ cm^{-1} lead to the total coupling strength of 2716 cm^{-1} in **C6ZA**, which is also consistent with the observed Soret band split (2578 cm^{-1}).

Excitation Energy Hopping in Z2 and 2Z2. Because the EEHs of **Z2** and **2Z2** are reversible between porphyrin units, a simple equilibrium scheme should be introduced as follows

$$\mathrm{Por}_A^*\mathrm{Por}_B \Leftrightarrow \mathrm{Por}_A\mathrm{Por}_B^*$$

where Por is the porphyrin unit, and k_1 and k_{-1} are forward and reverse reaction rate constants, respectively, which correspond to the EEH rate constants. Then, the EEH rate constants for the above reaction scheme can be defined by eq 7

$$\tau = \frac{1}{k_1 + k_{-1}} \tag{7}$$

where τ is the measured anisotropy decay times of **Z2** and **2Z2**. According to eq 7, the EEH rate constant via the 1,3-phenylene spacer of **2Z2** was determined to be 1.06×10^{11} s^{-1} (9.4 ps^{-1}) with $\tau = 4.7$ ps, while the EEH rate constant via direct linkage of **Z2** was determined to be 2.8×10^{12} s^{-1} (0.36 ps^{-1}) with $\tau = 0.18$ ps.

Excitation Energy Migration in C6ZA. The observed exciton−exciton annihilation and anisotropy depolarization strongly suggest the EEH phenomena in **C6ZA**. When the Förster-type incoherent energy hopping model is employed by assuming a migration-limited character of exciton−exciton annihilation and a random walk formalism of anisotropy decay, the analytical depolarization and exciton−exciton annihilation times are connected with the EEH time by eqs 8 and 9

$$\tau_{\text{depolarization}} = \frac{\tau_{\text{hopping}}}{4[1 - \cos^2(2\pi/N)]} = \frac{\tau_{\text{hopping}}}{4(1 - \cos^2\alpha)} \tag{8}$$

$$\tau_{\text{annihilation}} = \frac{N^2 - 1}{24}\tau_{\text{hopping}} \tag{9}$$

where N is the number of hopping sites, α the angle between the adjacent transition dipoles, $\tau_{\text{annihilation}}$ the slowest exciton−exciton annihilation time, and τ_{hopping} the inverse of the nearest-neighbor energy hopping rate.[21] Equation 8 is understood by considering that the depolarization is complete when the transition dipole migrates through 90° and by considering how many hops are required for this rotation to be accomplished. On the other hand, eq 9 assumes that the exciton−exciton annihilation reflects the migration-limited exciton−exciton recombination along the whole cyclic array and how many hops are required for this recombination to be accomplished.

The EEH time of **C6ZA** is calculated with the exciton−exciton annihilation and anisotropy decay times, given in Table 3 and Figure 7. Because **C6ZA** consists of six zinc(II) diporphyrin subunits, the number of hopping sites would be $N = 6$. Introducing $N = 6$ and $\alpha = 60°$ to eqs 8 and 9, the relations of $\tau_{\text{hopping}} = 3.00 \times \tau_{\text{depolarization}}$ and $\tau_{\text{hopping}} = 0.686 \times \tau_{\text{annihilation}}$ are obtained. As a consequence, the EEH time between the neighboring **Z2** subunits bridged by a 1,3-phenylene spacer is calculated to be 3.66 ps with the anisotropy decay time of 1.22 ps, given in Figure 7. In a different approach, the EEH time is evaluated to be 4.25 ps using the slowest exciton−exciton annihilation time of 6.2 ps, given in Table 3, where the slowest annihilation component[22] can describe the migration-limited exciton−exciton recombination along the wheel. It is noteworthy that the two different experimental observables, exciton−exciton annihilation and anisotropy depolarization times, result in a consistent EEH time (4.0 ± 0.4 ps) within a small error range. The excitation energy migration, thus, is well-described by the Förster-type incoherent energy hopping model, assuming the well-arranged cyclic system of **C6ZA**. It is noteworthy that **C6ZA** shows a faster EEH time (4.0 ± 0.4 ps) than 9.4 ps of linear **2Z2**. The accelerated hopping rate is rationalized in terms of the rigid geometry of **C6ZA**, in which the well-arranged and fixed porphyrin units have an advantage in dipole−dipole resonance as compared to the porphyrin units in random motions of linear **2Z2**.

Conclusions

We have investigated the excitation energy migration within a two-dimensional porphyrin wheel **C6ZA** that has six meso−meso linked zinc(II) diporphyrin (**Z2**) subunits bridged by 1,3-phenylene spacers. Both exciton−exciton annihilation and anisotropy depolarization effectively describe the excitation energy migration along **C6ZA**. Assuming the number of energy hopping sites $N = 6$, the two different experimental observables consistently give the EEH time of 4.0 ± 0.4 ps via a 1,3-phenylene spacer of **C6ZA**. The obtained EEH time is faster than that of linear porphyrin array **2Z2** because of a well-arranged and fixed circular geometry of the pigments. The faster EEH time of **C6ZA** is also rationalized in terms of strong exciton coupling strength resulting from the rigid molecular geometry. Overall, the investigation into the excitation energy migration of **C6ZA** affords a well-defined molecular model to understand the complicated excitation energy migration process occurring in natural light-harvesting systems.

Acknowledgment. The work at Yonsei was financially supported by the National Creative Research Initiatives Program of the Ministry of Science and Technology of Korea to D. Kim. The work at Kyoto was partly supported by a Grant-in-Aid from

the Ministry of Education, Culture, Sports, Science and Technology, Japan and 21st Century COE on Kyoto University Alliance for Chemistry to A. Osuka.

References and Notes

(1) van Oijen, A. M.; Ketelaars, M.; Köhler, J.; Aartsma, T. J.; Schmidt, J. *Science* **1999**, *285*, 400.

(2) (a) Sundström, V.; Pullerits, T.; van Grondelle, R. *J. Phys. Chem. B* **1999**, *103*, 2327. (b) Polivka, T.; Sundtröm, V. *Chem. Rev.* **2004**, *104*, 2021.

(3) van Grondelle, R.; Novoderezhkin, V. *Biochemistry* **2001**, *40*, 15057.

(4) Wasielewski, M. R. *Chem. Rev.* **1992**, *92*, 435.

(5) Gust, D.; Moore, T. A.; Moore, A. L. *Acc. Chem. Res.* **2001**, *34*, 40.

(6) Holten, D.; Bocian, D. F.; Lindsey, J. S. *Acc. Chem. Res.* **2002**, *35*, 57.

(7) Debreczeny, M. P.; Svec, W. A.; Marsh, E. M.; Wasielewski, M. R. *J. Am. Chem. Soc.* **1996**, *118*, 8174.

(8) Kodis, G.; Liddell, P. A.; de la Garza, L.; Clausen, P. C.; Lindsey, J. S.; Moore, A. L.; Moore, T. A.; Gust, D. *J. Phys. Chem. A* **2002**, *106*, 2036.

(9) (a) Kim, D.; Osuka, A. *Acc. Chem. Res.* **2004**, *37*, 735 and references therein. (b) Kim, D.; Osuka, A. *J. Phys. Chem. A* **2003**, *107*, 8791 and references therein. (c) Kim, Y. H.; Jeong, D. H.; Kim, D.; Jeoung, S. C.; Cho, H. S.; Kim, S. K.; Aratani, N.; Osuka, A. *J. Am. Chem. Soc.* **2001**, *123*, 76. (d) Cho, H. S.; Song, N. W.; Kim, Y. H.; Jeoung, S. C.; Hahn, S.; Kim, D.; Kim, S. K.; Yoshida, N.; Osuka, A. *J. Phys. Chem. A* **2000**, *104*, 3287. (e) Aratani, N.; Osuka, A.; Kim, D.; Kim, Y. H.; Jeong, D. H. *Angew. Chem., Int. Ed.* **2000**, *39*, 1458. (f) Kim, Y. H.; Cho, H. S.; Kim, D.; Kim, S. K.; Yoshida, N.; Osuka, A. *Synth. Met.* **2001**, *117*, 183. (g) Aratani, N.; Osuka, A.; Cho, H. S.; Kim, D. *J. Photochem. Photobiol. C: Photochem. Rev.* **2002**, *3*, 25. (h) Min, C.-K.; Joo, T.; Yoon, M.-C.; Kim, C. M.; Hwang, Y. N.; Kim, D.; Aratani, N.; Yoshida, N.; Osuka, A. *J. Chem. Phys.* **2001**, *114*, 6750. (i) Cho, H. S.; Jeong, D. H.; Yoon, M.-C.; Kim, Y.-R.; Kim, D.; Jeoung, S. C.; Kim, S. K.; Aratani, N.; Shinmori, H.; Osuka, A. *J. Phys. Chem. A* **2001**, *105*, 4200. (j) Jeong, D. H.; Yoon, M.-C.; Jang, S. M.; Kim, D.; Cho, D. W.; Yoshida, N.; Aratani, N.; Osuka, A. *J. Phys. Chem. A* **2002**, *106*, 2359. (k) Aratani, N.; Cho, H. S.; Ahn, T. K.; Cho, S.; Kim, D.; Sumi, H.; Osuka, A. *J. Am. Chem. Soc.* **2003**, *125*, 9668. (l) Yoon, M.-C.; Song, J. K.; Cho, S.; Kim, D. *Bull. Korean Chem. Soc.* **2003**, *24*, 1075. (m) Song, N. W.; Cho, H. S.; Yoon, M.-C.; Jeoung, S. C.; Yoshida, N.; Osuka, A.; Kim, D. *Bull. Korean Chem. Soc.* **2002**, *75*, 1023.

(10) (a) Yoshida, N.; Jeong, D. H.; Cho, H. S.; Kim, D.; Matsuzaki, Y.; Tanaka, K.; Osuka, A. *Chem.—Eur. J.* **2003**, *9*, 58. (b) Jeong, D. H.; Jang, S. M.; Hwang, I.-W.; Kim, D.; Yoshida, N.; Osuka, A. *J. Phys. Chem. A* **2002**, *106*, 11054. (c) Cho, H. S.; Song, J. K.; Ha, J.-H.; Cho, S.; Kim, D.; Yoshida, N.; Osuka, A. *J. Phys. Chem. A* **2003**, *107*, 1897. (d) Shinmori, H.; Ahn, T. K.; Cho, H. S.; Kim, D.; Yoshida, N.; Osuka, A. *Angew. Chem., Int. Ed.* **2003**, *42*, 2754.

(11) (a) Tsuda, A.; Osuka, A. *Science* **2001**, *293*, 79. (b) Cho, H. S.; Jeong, D. H.; Cho, S.; Kim, D.; Matsuzaki, Y.; Tanaka, K.; Tsuda, A.; Osuka, A. *J. Am. Chem. Soc.* **2002**, *124*, 14642. (c) Jeong, D. H.; Jang, S. M.; Hwang, I.-W.; Kim, D.; Matsuzaki, Y.; Tanaka, K.; Tsuda, A.; Nakamura, T.; Osuka, A. *J. Chem. Phys.* **2003**, *119*, 5237.

(12) (a) Choi, M.-S.; Yamazaki, T.; Yamazaki, I.; Aida, T. *Angew. Chem., Int. Ed.* **2004**, *43*, 150. (b) Choi, M.-S.; Aida, T.; Yamazaki, T.; Yamazaki, I. *Chem.—Eur. J.* **2002**, *8*, 2667. (c) Choi, M.-S.; Aida, T.; Luo, H.; Araki, Y.; Ito, O. *Angew. Chem., Int. Ed.* **2003**, *42*, 4060.

(13) (a) Officer, D. L.; Burrell, A. K.; Reid, D. C. W. *Chem. Commun.* **1996**, 1657. (b) Mak, C. C.; Bampos, N.; Sanders, J. K. M. *Angew. Chem., Int. Ed. Engl.* **1998**, *37*, 3020. (c) Solladie, N.; Gross, M.; Gisselbrecht, J.-P.; Sooambar, C. *Chem. Commun.* **2001**, 2206. (d) Biemans, H. A. M.; Rowan, A. E.; Verhoeven, A.; Vanoppen, P.; Latterini, L.; Foekema, J.; Schenning, A. P. H. J.; Meijer, E. W.; de Schryver, F. C.; Nolte, R. J. M. *J. Am. Chem. Soc.* **1998**, *120*, 11054. (e) Rucareanu, S.; Mongin, O.; Schuwey, A.; Hoyler, N.; Gossauer, A.; Amrein, W.; Hediger, H.-U. *J. Org. Chem.* **2001**, *66*, 4973. (f) Yeow, E. K. L.; Ghiggino, K. P.; Reek, J. N. H.; Crossley, M. J.; Bosman, A. W.; Schenning, A. P. H. J.; Meijer, E. W. *J. Phys. Chem. B* **2000**, *104*, 2596. (g) Taylor, P. L.; Wylie, A. P.; Huuskonen, J.; Anderson, H. L. *Angew. Chem., Int. Ed. Engl.* **1998**, *37*, 986.

(14) (a) McDermott, G. M.; Prince, S. M.; Freer, A. A.; Hawthonthwaite-Lawless, A. M.; Papiz, M. P.; Cogdell, R. J.; Isaacs, M. W. *Nature (London)* **1995**, *374*, 517. (b) Karrasch, S.; Bullough, P. A.; Ghosh, R. *EMBO J.* **1995**, *14*, 631. (c) Koepke, J.; Hu, X.; Muenke, C.; Schulten, K.; Michel, H. *Structure* **1996**, *4*, 581. (d) McLuskey, K.; Prince, S. M.; Cogdell, R. J.; Isaacs, N. W. *Biochemistry* **2001**, *40*, 8783. (e) Roszak, A. W.; Howard, T. D.; Southall, J.; Gardiner, A. T.; Law, C. J.; Isaacs, N. W.; Cogdell, R. J. *Science* **2003**, *302*, 1969. (f) Jungas, C.; Ranck, J.; Rigaud, J.; Joliot, P.; Vermeglio, A. *EMBO J.* **1999**, *18*, 534. (g) Ermler, U.; Fritzsch, G.; Buchanan, S.; Michel, H. *Structure* **1994**, *2*, 925.

(15) Nakamura, Y.; Hwang, I.-W.; Aratani, N.; Ahn, T. K.; Ko, D. M.; Takagi, A.; Kawai, T.; Matsumoto, T.; Kim, D.; Osuka, A. *J. Am. Chem. Soc.* in press.

(16) (a) Mongin, O.; Schuwey, A.; Vallot, M.-A.; Gossauer, A. *Tetrahedron Lett.* **1999**, *40*, 8347. (b) Anderson, S.; Anderson, H. L.; Sanders, J. K. M. *Acc. Chem. Res.* **1993**, *26*, 469. (c) Li, J.; Ambroise, A.; Yang, S. I.; Diers, J. R.; Seth, J.; Wack, C. R.; Bocian, D. F.; Holten, D.; Lindsey, J. S. *J. Am. Chem. Soc.* **1999**, *121*, 8927. (d) Biemans, H. A. M.; Rowan, A. E.; Verhoeven, A.; Vanoppen, P.; Latterini, L.; Foekema, J.; Schenning, A. P. H. J.; Meijer, E. W.; de Schryver, F. C.; Nolte, R. J. M. *J. Am. Chem. Soc.* **1998**, *120*, 11054. (e) Sugiura, K.; Fujimoto, Y.; Sakata, Y. *Chem. Commun.* **2000**, 1105. (f) Cho, H. S.; Rhee, H.; Song, J. K.; Min, C.-K.; Takase, M.; Aratani, N.; Cho, S.; Osuka, A.; Joo, T.; Kim, D. *J. Am. Chem. Soc.* **2003**, *125*, 5849.

(17) For a preliminary report of this work, see Peng, X.; Aratani, N.; Takagi, A.; Matsumoto, T.; Kawai, T.; Hwang, I.-W.; Ahn, T. K.; Kim, D.; Osuka, A. *J. Am. Chem. Soc.* **2004**, *126*, 4468.

(18) (a) Hwang, I.-W.; Kamada, T.; Ahn, T. K.; Ko, D. M.; Nakamura, T.; Tsuda, A.; Osuka, A.; Kim, D. *J. Am. Chem. Soc.* **2004**, *126*, 16187. (b) Hwang, I.-W.; Cho, H. S.; Jeong, D. H.; Kim, D.; Tsuda, A.; Nakamura, T.; Osuka, A. *J. Phys. Chem. B* **2003**, *107*, 9977. (c) Tsuda, A.; Nakamura, T.; Sakamoto, S.; Yamaguchi, K.; Osuka, A. *Angew. Chem., Int. Ed.* **2002**, *41*, 2817.

(19) Lewis, C.; Ware, W. R.; Doemeny, L. J.; Nemzek, T. L. *Rev. Sci. Instrum.* **1973**, *44*, 107.

(20) Wild, U. P.; Holzwarth, A. R.; Good, H. P. *Rev. Sci. Instrum.* **1977**, *48*, 1621.

(21) Bradforth, S. E.; Jimenez, R.; van Mourik, F.; van Grondelle, R.; Fleming, G. R. *J. Phys. Chem.* **1995**, *99*, 16179.

(22) (a) Trinkunas, G.; Herek, J. L.; Polívka, T.; Sundström, V.; Pullerits, T. *Phys. Rev. Lett.* **2001**, *86*, 4167. (b) Trinkunas, G. *J. Luminescence* **2003**, *102*, 532. (c) Brüggemann, B.; May, V. *J. Chem. Phys.* **2004**, *120*, 2325. (d) Müller, M. G.; Hucke, M.; Reus, M.; Holzwarth, A. R. *J. Phys. Chem.* **1996**, *100*, 9537. (e) Brüggemann, B.; Herek, J. L.; Sundström, V.; Pullerits, T.; May, V. *J. Phys. Chem. B* **2001**, *105*, 11391.

(23) Lakowicz, J. R. *Principles of Fluorescence Spectroscopy*, 2nd ed.; Kluwer Academic/Plenum Publishers: New York, 1999.

(24) (a) Kasha, M. *Radiat. Res.* **1963**, *20*, 55. (b) Kasha, M.; Rawls, H. R.; El-Bayoumi, M. A. *Pure Appl. Chem.* **1965**, *11*, 371. (c) Scholes, G. D.; Ghiggino, K. P. *J. Phys. Chem.* **1994**, *98*, 4580.

(25) Yatskou, M. M.; Koehorst, R. B. M.; Donker, H.; Schaafsma, T. J. *J. Phys. Chem. A* **2001**, *105*, 11425.